Journal of The Electrochemical Society, **146** (8) 2976-2982 (1999)
S0013-4651(98)11-075-3 CCC: $7.00

Reaction of Hydrogen/Water Mixtures on Nickel-Zirconia Cermet Electrodes

II. AC Polarization Characteristics

P. Holtappels,[a,z] I. C. Vinke, L. G. J. de Haart,* and U. Stimming*,[b]

Institut für Werkstoffe und Verfahren der Energietechnik, Teilinstitut 3: Energieverfahrenstechnik, Forschungszentrum Jülich, D-52425 Jülich, Germany

The impedance of nickel-zirconia cermet electrodes at the open-circuit potential was investigated as a function of temperature for different partial pressures of hydrogen and water. The impedance spectra for the hydrogen/water reaction show three apparent relaxation frequencies that are influenced by the temperature. The data are analyzed using an equivalent circuit representing two parallel reaction pathways which are attributed to (*i*) a reaction at the triple-phase boundary involving charge transfer and adsorption and (*ii*) a diffusion branch described by a resistor in series with a Warburg impedance. At temperatures below 890°C, a charge-transfer resistance dominates the real part of the impedance. A possible contribution of adsorption in the impedance spectra at higher temperatures is discussed. The diffusion branch is tentatively attributed to an electrochemical reaction in the area of the nickel/electrolyte interface, which is limited by diffusion of protons in the electrolyte phase. The activation enthalpy calculated for this process is between 120 and 160 kJ mol^{-1}.

Manuscript submitted November 24, 1998; revised manuscript received March 24, 1999.

For investigating the dynamics of electrochemical reactions, impedance spectroscopy proves to be a powerful tool in determining the number and kind of processes involved in the interfacial reaction.[1] The interpretation of the impedance spectra needs to separate complex contributions of non-faradaic processes, *e.g.*, the charging of the electrochemical double layer, from contributions of the electrochemical reaction, which is the faradaic impedance,[2] Z_F. The faradaic impedance can give information on the processes involved in the electrochemical reaction.

Impedance spectra reported previously for nickel-zirconia (Ni-YSZ) cermet electrodes are rather complex and, obviously, influenced by more than one process.[3-8] The influence of the cermet preparation and structure[3-6] as well as contributions of the gas atmosphere above the cermet electrode have been investigated.[7] Mechanistic models have also been proposed and correlated to the impedance data.[8-10] The results are, however, not always fully understood, but they indicate a complex correlation between preparation, structure, and prehistory of the Ni-YSZ cermet electrode, the experimental setup, and the corresponding impedance. The study of these relationships might be complicated by the fact that complex electrochemical kinetics have been suggested for the hydrogen/water reaction at even simpler shaped Ni-cone electrodes.[11]

In this work, impedance data are presented for a single kind of Ni-YSZ cermet electrodes, which have been characterized by dc measurements. The dc polarization characteristics are described in Part I[12] and indicate different electrochemical kinetics for the hydrogen oxidation and the hydrogen evolution reaction. A charge-transfer controlled reaction rate was concluded for the hydrogen oxidation reaction in the temperature range from 725 to 845°C. Adsorption was indicated for this reaction at temperatures above 890°C and might affect the hydrogen evolution reaction as well. Based on these results and literature data for the Ni/YSZ system, a model is developed describing possible processes in the investigated Ni-YSZ cermet electrodes.

Experimental

The electrodes consist of annular-shaped Ni-YSZ cermet and $La(Sr)MnO_3$ perovskite electrodes screen-printed as symmetrically as possible on each side of 150 μm thick electrolyte disks. Zirconia stabilized with 8 mol % yttria (8YSZ) was used as the electrolyte and as the ceramic phase in the Ni-YSZ cermet electrodes. The inner and outer diameters of the electrodes were 4 and 12 mm, respectively, giving a geometric area of 1 cm^2. Pt mesh current collectors were pressed in contact to the electrodes. A spring-loaded Pt point contact in the center of the cathode served as the reference electrode. The experimental setup has been described previously.[12] The reliability of this cell design in dc and ac polarization measurements has been verified by modeling of the cell current-potential distribution considering the in-plane conductivity, the sloping edges, and the electrochemical properties of both the working and the counter electrode.[13]

The fuel compartment was flushed with a mixture of H_2, H_2O, and Ar with a total flow of 200-250 mL min^{-1}. Analogue mass flow controllers (Brooks 5850) regulated the flow of H_2 and Ar. The H_2/Ar mixture was saturated with water at controlled temperatures. Measurements were performed in three gas atmospheres (*i*) p_{H_2} = 0.48 bar/p_{H_2O} = 0.12 bar, (*ii*) p_{H_2} = 0.48 bar/p_{H_2O} = 0.05 bar, and (*iii*) p_{H_2} = 0.19 bar/p_{H_2O} = 0.05 bar, the balance to 1 bar being Ar. The temperature range was 725 to 950°C.

Impedance measurements were performed at the open-circuit potential (OCP) in the frequency range from 20 kHz to 0.05 Hz using a Solartron 1255 FRA in combination with a Bank LB81M potentiostat. The amplitude was 20 mV. The data were analyzed using the program EQUIVCRT.[14]

The microstructure of the Ni-YSZ cermet electrodes was investigated after the electrochemical testing by optical microscopy. The samples were embedded into epoxy, cut, ground, and polished with diamond paste (1 μm). Pictures were obtained from the polished cross sections of the samples.

Impedance Model

Microstructure.—A representative microstructure of a Ni-YSZ cermet electrode is given in Fig. 1. Light areas representing the Ni phase can clearly be distinguished from the YSZ phase and pores, related to the gray and dark gray areas, respectively. The Ni grain size is estimated to be in the range of 0.5-3 μm, the YSZ grains and the pore diameters are 0.5-10 μm. For the above described electrode structure a reaction model is developed on the basis of the steady state results and literature data for the Ni/YSZ system.

Reaction model.—As concluded from the dc polarization characteristics, the rate of the hydrogen oxidation reaction with oxygen ions is considered to be controlled by charge transfer and possibly by

* Electrochemical Society Active Member.
[a] Present address: Materials Research Department, Risø National Laboratory, DK-4000, Roskilde, Denmark.
[b] Present address: Physik-Department E19, Technische Universität München, D-85748 Garching, Germany.
[z] E-mail: peter.holtappels@risoe.dk

S0013-4651(98)11-075-3 CCC: $7.00

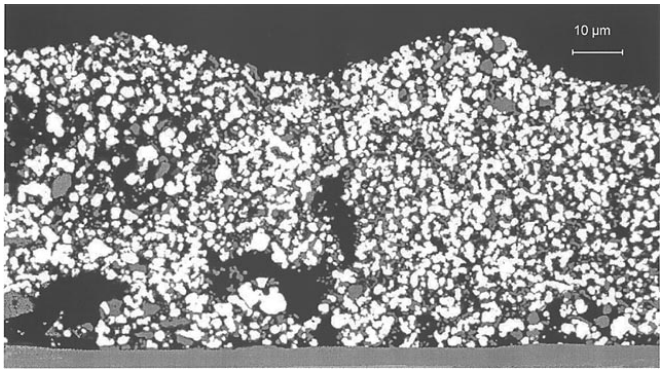

Figure 1. Microscopic image showing the cross section of a screen printed Ni-YSZ cermet electrode.

adsorption on the Ni surface. The overall electrochemical reaction involves species in the gas phase, the electrolyte, and on the Ni surface, and thus may take place in a certain area around the triple-phase boundary line (TPL). Because of the permeability of hydrogen in Ni [15] and certain proton conductivity in the YSZ,[16] an electrochemical reaction in the area of the Ni/YSZ interface is possible as suggested earlier by Chebutin *et al.*[17] The reactions at both the TPL and the Ni/YSZ interface may contribute to the faradaic current. Possible reaction steps are illustrated in Fig. 2. The first step is considered to be the dissociative adsorption of H_2 on Ni. Two different reaction pathways are assumed for the oxidation of the adsorbed hydrogen atoms and are discussed as follows. On the gas exposed Ni surface and in the region of the TPL, H_{ad} can be oxidized in the presence of oxygen ions from the electrolyte. Subsequently, the water formation reaction may proceed via intermediates, *e.g.*, hydroxides on the Ni surface.[12] In the area of the Ni/YSZ interface, hydrogen dissolved in Ni, denoted H_{Ni}, may be oxidized by forming interstitial protons, $H_i^{\bullet}$, or hydroxides, $OH_O^{\bullet}$, in the electrolyte. The transport of H_{Ni} and $H_i^{\bullet}$ [16] may occur via diffusion in the Ni and the electrolyte phase, respectively. The remaining processes, *e.g.*, formation, dissociation, as well as adsorption and desorption of water might take place in the triple-phase boundary region. Gas transport limitations are not considered because of the porosity of the Ni-YSZ cermet electrode and the high binary diffusion coefficients of the hydrogen/water mixtures.[18]

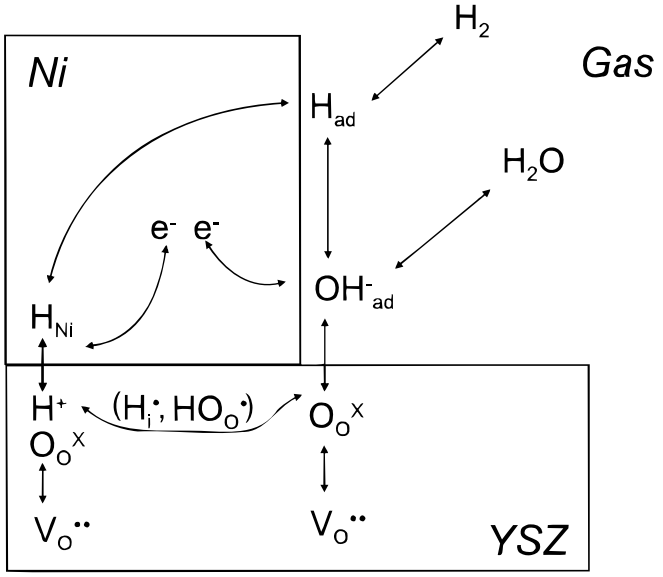

Figure 2. Model for the electrochemical reaction of gaseous hydrogen and water at the triple-phase boundary and in the area of the Ni/YSZ interface in a Ni-YSZ cermet electrode.

Faradaic reaction around the TPL.—As illustrated in the reaction model in Fig. 2, two processes, charge transfer and adsorption, are considered in the hydrogen water reaction around the TPL. A Butler–Volmer type equation, resulting in an exponentially increasing current at high overpotentials, can describe the rate of the charge-transfer reaction. As concluded from the dc polarization characteristics[12] the reaction rate may be influenced by adsorption especially at high temperatures. If the exchange rates in the charge-transfer and adsorption reaction are high, large current densities can be expected for the triple-phase boundary reaction.

Faradaic reaction in the area of the Ni/YSZ interface.—The reaction in the area of the Ni/YSZ interface may involve charge-transfer across the interface as well as transport of H_{Ni} and $H_i^{\bullet}$ to and away from the Ni/YSZ interface, respectively. Assuming that mass transport occurs only via diffusion, limiting currents according to Ficks law Eq. 1, can be estimated by an order of magnitude calculation as done by Mogensen *et al.*[19]

$$j_{\mathrm{lim,i}} = nFD_{\mathrm{i}} \frac{\Delta C_{\mathrm{i}}}{\Delta x} \qquad [1]$$

For species i (i = H_{Ni}, $H_i^{\bullet}$) the diffusion coefficient, D_i, can be taken from the literature and is given in Table I. In a simple approach, the Ni grains are considered as ideal half-spheres and the diffusion length Δx is assumed to be the radius of the Ni grains. From Fig. 1, values between 0.25 and 1.5 µm are estimated for Δx. The concentration gradient ΔC_i might be between 10 and 100% of the saturation concentration of the diffusing species. Inserting these values in (*i*) provides limiting currents between 0.07 and 4.2 mA cm^{-2} for the proton diffusion in YSZ at 986°C and $p_{H_2O} = 0.024$. In contrast, limiting currents higher than 1 A cm^{-2} are calculated for the hydrogen diffusion in Ni. Comparing the diffusion rates of atomic hydrogen in Ni and protons in YSZ it is clear to see that, the hydrogen reaction in the area of the Ni/YSZ interface will be limited by the transport of protons in the electrolyte.

The measured current densities of the hydrogen/water reaction at 950°C and $p_{H_2} = 0.48$ bar/$p_{H_2O} = 0.05$ bar are 41 ± 1 mA cm^{-2} at $|\eta| = 20$ mV anodic and cathodic overpotential.[12] This current density is higher than the limiting current calculated for the proton diffusion in YSZ. Considering that the measurement temperature is lower than the expected temperatures for the literature data, it is likely that the hydrogen reaction in the area of the Ni/YSZ interface does not contribute significantly to the total stationary faradaic current sustained by the reaction around the TPL. We can further conclude that (*i*) water formation and desorption may not play an important role in the reaction in the area of the Ni/YSZ interface and (*ii*) the triple-phase boundary reaction will not significantly be disturbed by species involved in this additional reaction pathway. Presuming a fast charge-transfer rate in the area of the Ni/YSZ interfacial region, limiting conditions for proton diffusion may be reached also at small polarization, *e.g.*, in impedance measurements at OCP.

Table I. Saturation concentration, diffusion coefficient, and corresponding limiting currents according to Fick's law for hydrogen dissolved in Ni and protons in YSZ.

	H_{Ni} in Ni (1000°C)	$H_i^{\bullet}$ in YSZ (986°C)
C_0 (mol cm^{-3})	$1.1 \cdot 10^{-4}$ (Ref. 19)	$9.9 \cdot 10^{-7}$ (Ref. 19)
D_H (cm^2 s^{-1})	$1.5 \cdot 10^{-4}$ (Ref. 15)	$1.1 \cdot 10^{-6}$ (Ref. 16)
j_{lim} (mA cm^{-2})	1060	0.07
ΔC = 10% $C_{0,i}$		
Δx = 1.5 µm		
j_{lim} (mA cm^{-2})	63700	4.2
ΔC = $C_{0,i}$		
Δx = 0.25 µm		

S0013-4651(98)11-075-3 CCC: $7.00

Overall impedance model.—A general description of the impedance of each of the individual reaction pathways can be found in the literature.[1,2,20] The equivalent circuit describing an electrochemical reaction involving charge-transfer and adsorbed species is given in Fig. 3a. Therein, R_{CT} represents the charge-transfer resistance. The parameters R_P and Q_P describe the time constant for changing the degree of coverage of at least one adsorbed specie on the electrode surface that follow the charge-transfer reaction.[21,22]

The equivalent circuit describing a diffusion-controlled electrode reaction is the Randles-type circuit given in Fig. 3b. Therein, R_W describes the charge transfer in the area of the Ni/YSZ interface. $Z_{W\infty}$ is the Warburg impedance related to mass transport via linear diffusion. The Warburg impedance applies as well for a spherical diffusion of protons in YSZ and in the frequency range investigated. The Randles circuit may be correlated with the hydrogen reaction in the area of the Ni/YSZ interface. In Fig. 3a and b the charging of the double layer, C_{DL}, is also considered.

Both the triple-phase boundary reaction and the reaction in the area of the Ni/YSZ interface, may occur independently of each other, and consequently they have to be described as parallel reaction pathways. Setting the equivalent circuits Fig. 3a and b in parallel results in c. Now, the real part of the faradaic impedance is determined by charge transfer and adsorption around the TPL, which are described by the resistances R_{CT} and R_P, respectively. The complex part of the faradaic impedance is determined by the parameters R_W, W, and Q_P and thus is clearly affected by both reaction pathways. The complex part is also influenced by the charging of the electrochemical double layer, C_{DL}.

The analysis shows that impedance spectra containing up to three time constants can be expected for the reaction of hydrogen and water at a single Ni/YSZ contact point. The Ni/YSZ cermet structure shown in Fig. 1 can be described as a dispersion of these contact points. Based on the assumptions that because of sufficient percolation of the electronically conducting Ni phase (*i*) the electrochemically active area in the Ni-YSZ cermet electrode is restricted to a few micron thick layer toward the solid YSZ/Ni-YSZ cermet interface and (*ii*) further contributions of the bulk of the cermet electrodes can be excluded in the impedance, the reaction model Fig. 2 may, indeed, be applied to the investigated Ni-YSZ cermet electrodes. From the reaction model it is evident that structural parameters, *e.g.*, particle size and distribution will have an influence on the resulting impedance by changing the ratios between the length of the TPL, the area of the Ni/YSZ interface, and the gas-exposed surface area. Previously reported impedance spectra[6] that are obviously influenced by the microstructure of the Ni-YSZ cermet electrodes are not contradicting the above discussed reaction model.

The corresponding equivalent circuit Fig. 3c was used to describe the impedance at OCP in the temperature range from 725 to 950°C for the three gas atmospheres investigated. The ohmic resistance, R_Ω, and the inductance, L, are related to the ohmic losses in the test circuit and inductive contributions of the measurement system, respectively, and do not belong to the interfacial reaction. Impedance spectra shown in this work are already corrected for R_Ω and L.

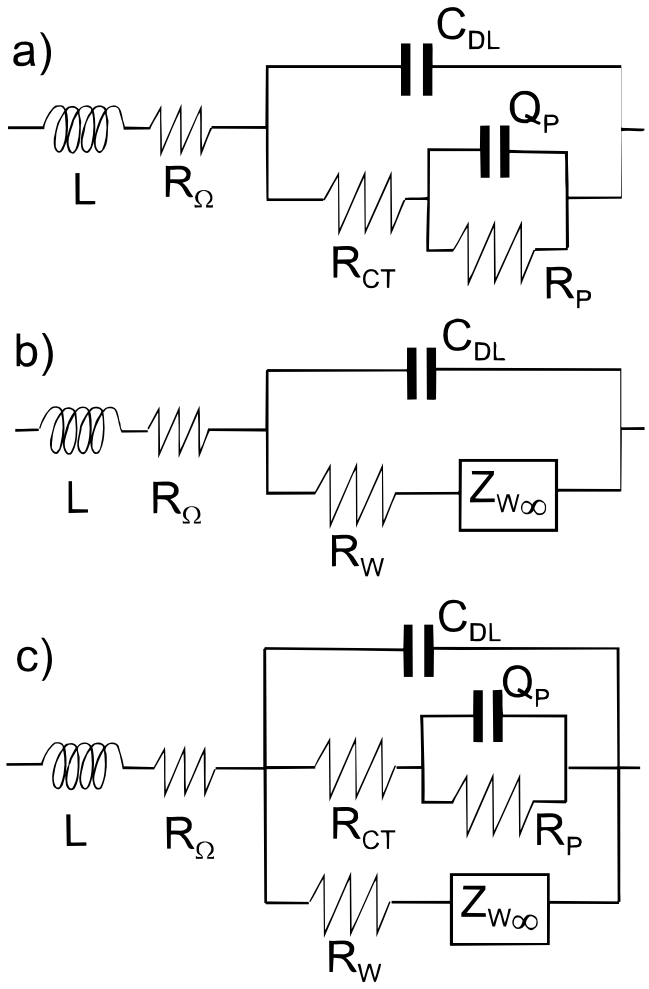

Figure 3. Equivalent circuits derived from the reaction model Fig. 2: (a) electrochemical reaction controlled by charge transfer and adsorption, (b) electrochemical reaction controlled by diffusion, (c) overall equivalent circuit for a parallel arrangement of (a) and (b).

Results and Discussion

Impedance spectra.—Figure 4 shows the influence of temperature on the impedance at OCP at constant $p_{H_2} = 0.48$ bar and $p_{H_2O} = 0.05$ bar. In the temperature range from 725 to 890°C, three maxima, denoted f_1, f_2, and f_3, are observed in the imaginary part. The frequency at the mid maximum f_2 increases continuously from 10 to 500 Hz with increasing temperature. The frequency at f_1 increases from 725 to 845°C but decreases again at higher temperatures. The frequency for the maximum f_3 is not as clear to distinguish as for f_1 and f_2, but may be on the same order of magnitude as f_2 at 950°C.

The lines in Fig. 4 represent the simulation using the equivalent circuit in Fig. 3c. The relative error in the real and imaginary part is below 2% at all experimental conditions. These relative errors are fairly low and a satisfactory agreement between measurement and simulation is obtained for all three gas atmospheres in the temperature range investigated.

The processes attributed to the apparent relaxation frequencies, f_1 to f_3, are analyzed in the admittance plane by plotting the imaginary part of the admittance *vs.* the real part. The parallel processes appear

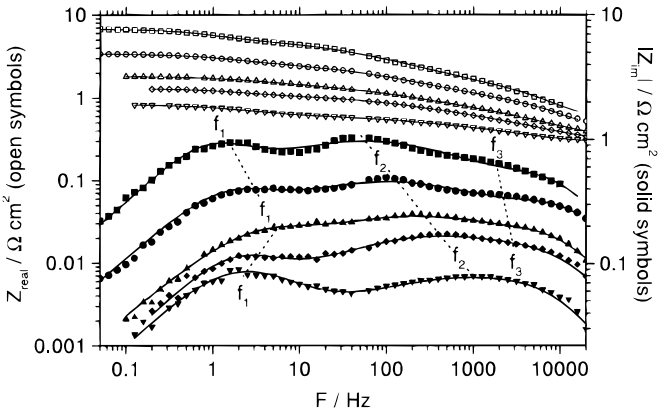

Figure 4. Bode-Z plot of the impedance spectra at OCP as a function of temperature for $p_{H_2} = 0.48$ bar and $p_{H_2O} = 0.05$ bar; open symbols represent the real part, Z_{real}; solid symbols represent the imaginary part, Z_{im}; (a) (□) 725°C, (b) (○) 780°C, (c) (△) 845°C, (◇) 890°C, (▽) 950°C, (—): simulation using the reaction model Fig. 3c.

S0013-4651(98)11-075-3 CCC: $7.00

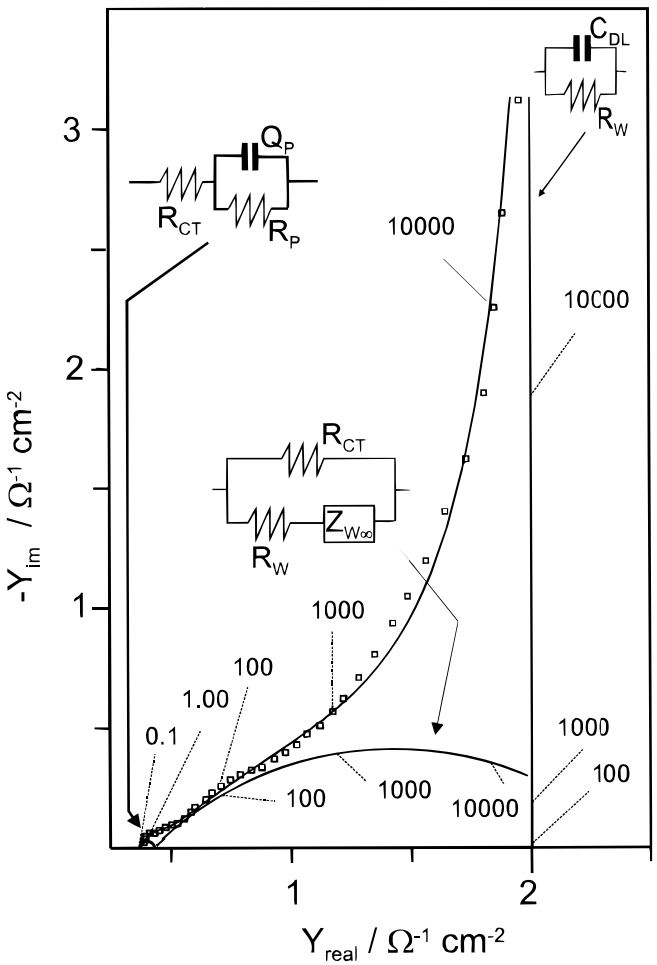

Figure 5. Admittance plot of the impedance spectra at OCP; T = 780°C, p_{H_2} = 0.48 bar, p_{H_2O} = 0.05 bar, (□) measurement, (—) simulation using the reaction model Fig. 3c; numbers indicate the frequencies in hertz.

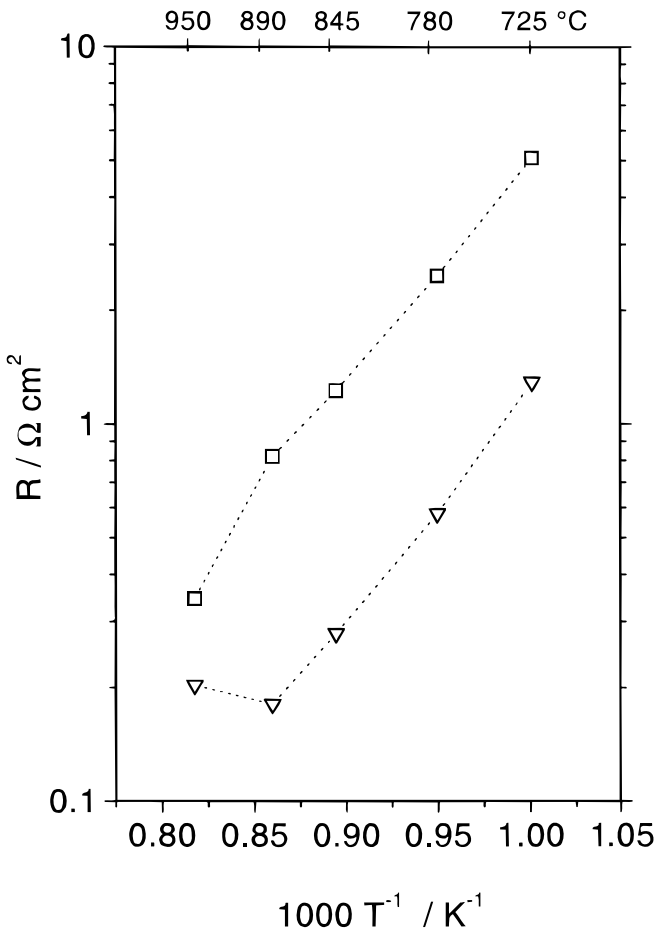

Figure 6. Reaction model parameters R_{CT} (□) and R_p (▽) as a function of temperature at OCP; p_{H_2} = 0.48 bar, p_{H_2O} = 0.05 bar.

sequentially in the admittance plot ($1/Z^*$) in Fig. 5. At frequencies above 10 kHz, the charging of the capacitance C_{DL} across the resistance R_W dominates the spectrum. In a medium frequency region down to 10 Hz, the series of R_W and W in parallel to the resistor R_{CT} determine the frequency distribution. Below 1 Hz, the parameters R_{CT}, R_P, and Q_P describe the admittance. The equivalent circuit parameters are discussed in detail below.

The parameters R_{CT}, R_P, and Q_P describing the TPL reaction.—Figure 6 shows the values for the model parameters R_{CT} and R_P as a function of temperature for p_{H_2} = 0.48 bar and p_{H_2O} = 0.05 bar. In the temperature region from 725 to 890°C R_{CT} is significantly higher than R_P. Above 890°C, R_P changes its temperature dependence and remains almost constant with increasing temperature. The real part of the faradaic impedance, R_F, is the sum of R_{CT} and R_P and thus is dominated by R_{CT} in the temperature range from 725 to 890°C. At 950°C, both R_{CT} and R_P contribute significantly to R_F. Therefore, the results indicate a charge-transfer controlled electrode reaction at low temperatures.

According to the low field approximation of the Butler-Volmer Eq. 2 the reciprocal charge-transfer resistance at low overpotentials is proportional to the exchange current density, j_0

$$j_0 = \frac{R}{nF} \cdot \frac{T}{R_{CT}} \qquad [2]$$

As R_{CT} is attributed to a charge-transfer resistance, the temperature dependence of j_0 can be obtained by plotting the quantity T/R_{CT} as a function of temperature. This is done in Fig. 7 for the three gas atmospheres investigated. T/R_{CT} shows Arrhenius behavior with an activation enthalpy of 130 and 150 kJ mol^{-1} for high and low hydrogen partial pressures, respectively. These values show a close resemblance to the activation enthalpy of the steady-state hydrogen oxidation reaction at OCP [12] which was found to be charge-transfer controlled at low temperatures.

At 950°C, a second contribution described by the parameters R_P and Q_P in addition to the charge-transfer process has to be considered. As is seen in Fig. 8, Q_P increases exponentially with temperature up to 890°C, but is less dependent on temperature above 890°C. The exponent n_P of the constant phase element Q_P is between 0.8 and 1 and not clearly affected by the temperature. The highest values for Q_P are observed for p_{H_2} = 0.48 bar and p_{H_2O} = 0.12 bar, which are the highest partial pressures investigated. The temperature dependence of R_P and Q_P below 890°C and the fact that R_P is not influenced by the hydrogen partial pressure at 950°C rule out gas conversion[7] from determining the low frequency process. Rather, these results agree with the assumption that at high temperatures there is a high fractional surface coverage at temperatures above 890°C. For these temperatures, a significant contribution of adsorption due to a limited number of available adsorption sites was also indicated in the dc polarization characteristics.

Both the ac and the dc polarization characteristics are in accordance with a charge-transfer controlled electrode reaction at temperatures below 890°C. At higher temperatures most likely two processes, charge transfer and adsorption, determine the rate of the overall electrode reaction. From this mutual agreement it is concluded that the equivalent circuit Fig. 3c is valid for describing the impedance of the Ni-YSZ cermet electrodes at *OCP* in H_2/H_2O atmospheres. As

S0013-4651(98)11-075-3 CCC: $7.00

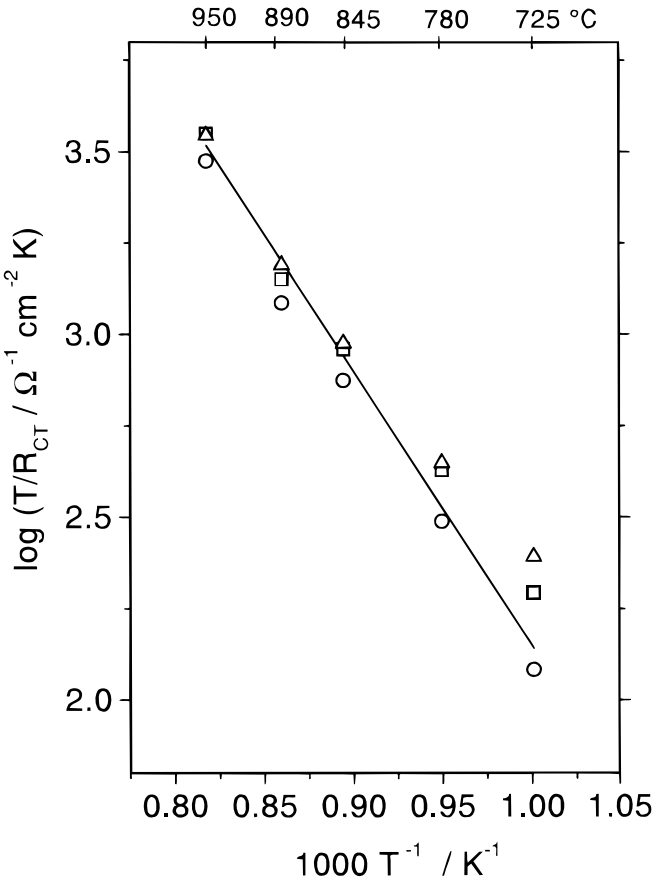

Figure 7. Temperature dependence of T/R_{CT} at *OCP*: (○) p_{H_2} = 0.19 bar, p_{H2O} = 0.05 bar, (□) p_{H_2} = 0.48 bar, p_{H2O} = 0.05 bar, (△) p_{H_2} = 0.48 bar, p_{H2O} = 0.12 bar, line corresponds to a slope of 145 kJ mol^{-1}.

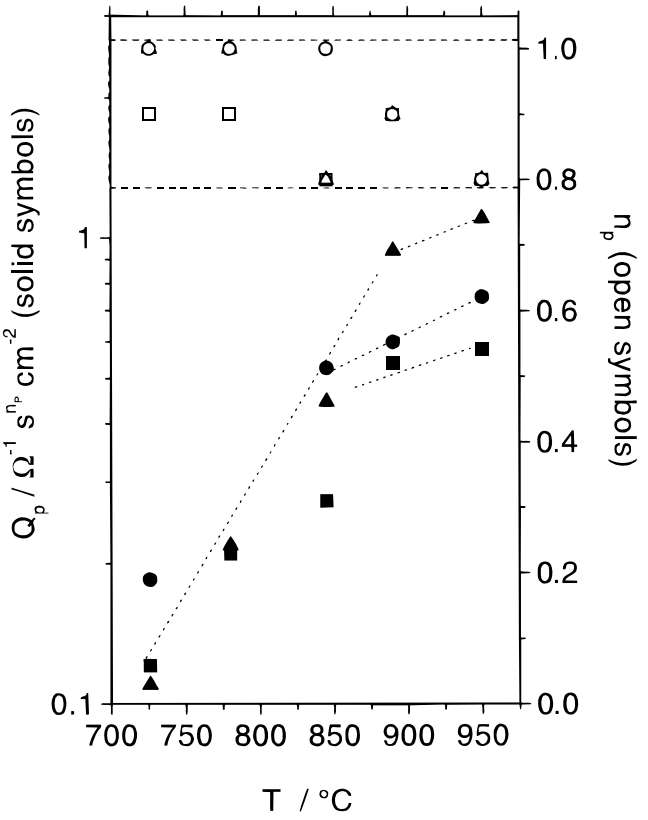

Figure 8. Reaction model parameter Q_p (solid symbols) and corresponding exponent n_p (open symbols) as a function of temperature at *OCP*: (●, ○) p_{H_2} = 0.19 bar, p_{H2O} = 0.05 bar; (■, □) p_{H_2} = 0.48 bar, p_{H2O} = 0.05 bar, (▲, △) p_{H_2} = 0.48 bar, p_{H2O} = 0.12 bar.

shown in Fig. 5, charge transfer and adsorption, attributed to the electrochemical reaction at the TPL, contribute to the low frequency part of the impedance. The parameters, C_{DL}, R_W, and W, affecting the impedance at higher frequencies are discussed below.

The capacitance C_{DL}.—The experimentally obtained values for C_{DL} are given in Table II. In the low temperature region (725-845°C), C_{DL} amounts to 21 to 64 μF cm^{-2}. The capacitance, C_{DL}, might be in general related to the differential double-layer capacitance at the electrode/electrolyte interface. Values reported for this capacitance at the Pt/YSZ interface[23,24] and for Au electrodes on YSZ single crystals[25] are 0.5-14 μF cm^{-2} and 20-40 μF cm^{-2}, respectively, and thus, in the same order of magnitude as the values for C_{DL}. Considering additionally the rough and inhomogeneous structure of the Ni-YSZ cermet electrodes close to the solid electrolyte, C_{DL} may be related to the double-layer capacitance in the Ni-YSZ/YSZ system.

The parameters R_W and W describing the diffusion branch.—The charging of the double-layer capacitance starts via the resistance R_W. Considering R_W as a charge-transfer resistor and according to Eq. 3 the values for T/R_W are plotted in Fig. 9 as a function of temperature for the different gas atmospheres. T/R_W shows Arrhenius behavior with an activation enthalpy of 110 ± 5 kJ mol^{-1}. In the low temperature region T/R_W is almost independent of the gas atmosphere.

At intermediate frequencies down to 10 Hz, the Warburg impedance contributes significantly to the frequency distribution. The Warburg impedance, $Z_{W\infty}$, can be described by the Warburg element, W. At 950°C, the experimental values for W range from 0.009 to 0.049 A V^{-1} s$^{0.5}$ cm^{-2} depending on the gas atmosphere (see Table III).

From the definition of W Eq. 3 [20]

$$W = \frac{n^2F^2\sqrt{2}}{RT}\left(\frac{1}{C^*_{Ox}\sqrt{D_{Ox}}} + \frac{1}{C^*_{Red}\sqrt{D_{Red}}}\right) \qquad [3]$$

the Warburg element is determined by the diffusion coefficient D_i and the concentration C_i^* of the diffusing species i involved in the electrochemical reaction. According to the model, the indexes Ox and Red in Eq. 3 refer to $H_i^\bullet$ and H_{Ni}, respectively. Because both C_i^* and D_i are much higher for the hydrogen dissolved in Ni (see Table I) the term in the parenthesis in Eq. 3 is likely to be determined by the diffusion of protons in the electrolyte, Eq. 4

$$\left(\frac{1}{C^*_{H_i^\bullet}\sqrt{D_{H_i^\bullet}}} + \frac{1}{C^*_{H_{Ni}}\sqrt{D_{H_{Ni}}}}\right)^{-1} \approx C^*_{H_i^\bullet}\sqrt{D_{H_i^\bullet}} \qquad [4]$$

Table II. Capacitance C_{DL} as function of temperature for different gas atmospheres.

T (°C)	C_{DL} (μF cm^{-2}) p_{H_2} = 0.19 bar p_{H2O} = 0.05 bar	C_{DL} (μF cm^{-2}) p_{H_2} = 0.48 bar p_{H2O} = 0.05 bar	C_{DL} (μF cm^{-2}) p_{H_2} = 0.48 bar p_{H2O} = 0.12 bar
725	21	31	22
780	26	41	30
845	55	64	63
890	76	41	59
950	194	61	111

S0013-4651(98)11-075-3 CCC: $7.00

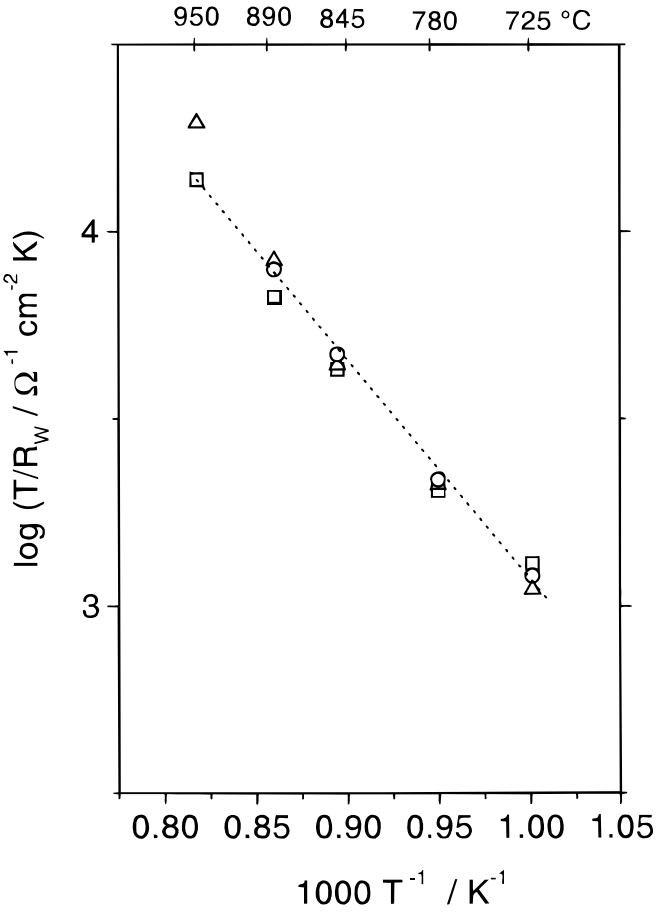

Figure 9. Temperature dependence of T/R_W at *OCP*: (○) p_{H_2} = 0.19 bar, p_{H_2O} = 0.05 bar; (□) p_{H_2} = 0.48 bar; p_{H_2O} = 0.05 bar; (△) p_{H_2} = 0.48 bar, p_{H_2O} = 0.12 bar; line corresponds to a slope of 110 kJ mol^{-1}.

The calculated and experimentally obtained values for W are given in Table III. For the proton diffusion in YSZ, calculated and experimentally obtained values for W are of the same order of magnitude. Therefore, W might be related to the proton diffusion in YSZ, which limits the rate of the hydrogen reaction in the area of the Ni/YSZ interface. This is also supported by the result that the charge-transfer resistance R_W is nearly independent of the gas atmosphere.

As shown, the model parameters C_{DL}, R_W, and W may, indeed, be related to processes in the area of the Ni/YSZ interface which are the charging of the double layer, the charge transfer in the area of the Ni/YSZ interface, and the proton diffusion in YSZ, respectively. The analysis shows that the impedance spectra are well described by the equivalent circuit Fig. 3c correlated with processes around a single Ni/YSZ contact point on a micrometric scale. Additional contributions arising from the bulk of the cermet structure[10] cannot be resolved. Therefore, we conclude that the impedance of the hydrogen/water reaction is determined by two independent processes which are charge-transfer coupled with adsorption at the TPL and proton diffusion in the YSZ electrolyte in the area of the Ni/YSZ interface.

Table III. Warburg element *W* obtained from experiments and calculated for proton transport in YSZ and for hydrogen transport in Ni.

	T (°C)	W (A V^{-1} s$^{0.5}$ cm^{-2})
Experimental	950	0.009-0.049
$H_i^{\bullet}$ in YSZ	986	0.0038
H_{Ni} in Ni	1000	4.3

The temperature dependence of the proton diffusion in zirconia stabilized with 8 mol % yttria can be found by analyzing the temperature dependence of the Warburg element W. Inserting Eq. 4 in Eq. 3 yields expression 5 for the average diffusion coefficient of this process

$$D_{H_i^{\bullet}} \approx \left(\frac{R^2}{2n^4F^4} \cdot \frac{1}{C^{*2}_{H_i^{\bullet}}} \right) \cdot W^2 \cdot T^2 \qquad [5]$$

Presuming that the saturation concentration of protons in 8YSZ is independent of temperature, the product $W^2 \cdot T^2$ is proportional to the average diffusion coefficient of these species. The temperature dependence of the quantity $W^2 \cdot T^2$ is shown in Fig. 10. The values for $W^2 \cdot T^2$ increase with decreasing hydrogen partial pressure and increasing water content at temperatures between 725 and 845°C. For this temperature region, a linear dependency can be observed in the Arrhenius plots. The activation enthalpy of the proton diffusion in 8YSZ is between 120 and 160 kJ mol^{-1} depending on the gas atmosphere. To our knowledge, the activation enthalpy of this process and its dependence on p_{H_2}, p_{H_2O}, and p_{O_2} has not been previously determined experimentally.

At temperatures above 845°C, the values for $W^2 \cdot T^2$ as well as the simulation parameters R_W and C_{DL} scatter significantly. Two reasons may account for this: (*i*) at 950°C, the high frequency and mid-frequency maxima, f_2 and f_3, and thus the corresponding processes cannot be separated sufficiently (see Fig. 4) and (*ii*) at temperatures above 890°C, the inductance of the measurement system affects the impedance spectra at frequencies below 10 kHz, which is almost the relaxation frequency for the charging of C_{DL} across R_W. Therefore,

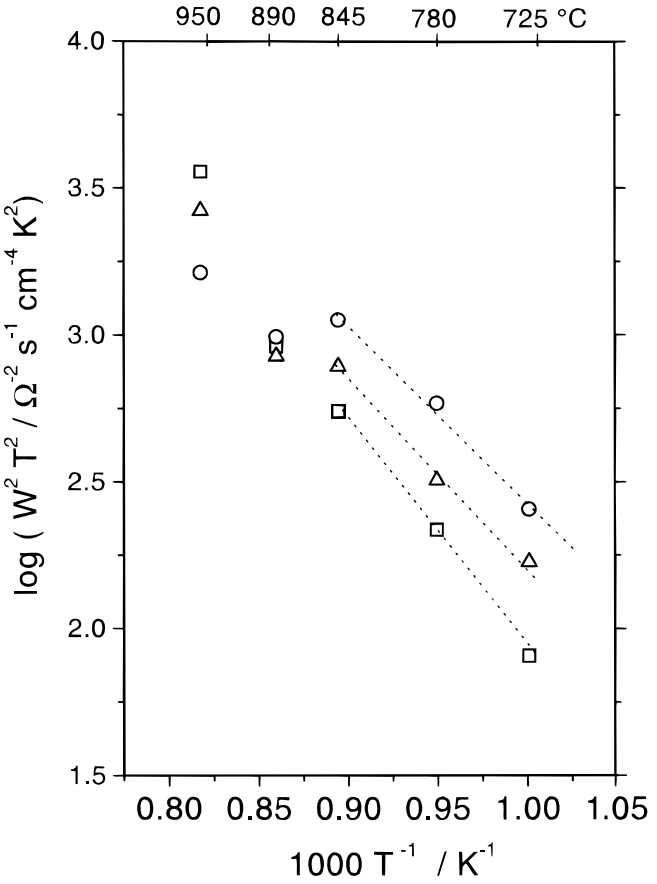

Figure 10. Temperature dependence of $W^2 \cdot T^2$ at *OCP*: (○) p_{H_2} = 0.19 bar, p_{H_2O} = 0.05 bar; (□) p_{H_2} = 0.48 bar, p_{H_2O} = 0.05 bar; (△) p_{H_2} = 0.48 bar, p_{H_2O} = 0.12 bar.

S0013-4651(98)11-075-3 CCC: $7.00

higher uncertainties are expected for R_W, W, and C_{DL} at temperatures above 845°C compared to lower temperatures.

Conclusions

The impedance of the hydrogen/water reaction on Ni-YSZ cermet electrodes at the open-circuit potential involves up to three processes with different dependencies on temperature and the partial pressure of the reactants. At temperatures below 845°C, the real part of the faradaic impedance was found to be charge-transfer controlled. The activation enthalpy of the charge transfer resistance, R_{CT}, shows close resemblance to the activation enthalpy of the steady-state hydrogen oxidation reaction at *OCP*. At temperatures above 890°C, two reaction steps, charge transfer and adsorption due to a high fractional surface coverage, determine the overall reaction rate.

The complexities of the impedance spectra may result from the charging of the electrochemical double layer and a parallel reaction, which is limited by diffusion. The results agree with the assumption that this is the hydrogen reaction in the area of the Ni/YSZ interface, which is limited by the diffusion of protons in the electrolyte.

Research Center Juelich, Institut fuer Werkstoffe und Verfahren der Energietechik, assisted in meeting the publication costs of this article.

References

1. M. Sluyters-Rehbach and J. H. Sluyters, in *Electroanalytical Chemistry, A Series of Advances*, Vol. 4, A. J. Bard, Editor, p. 3, Marcel Dekker, New York (1970).
2. M. Sluyters-Rehbach and J. H. Sluyters, in *Comprehensive Treatise of Electrochemistry*, Vol. 9, E. Yeager, J. O'M. Bockris, B. E. Conway, and S. Sarangapani, Editors, p. 177, Plenum Press, New York (1984).
3. M. E. Seiersten, P. H. Middleton, and B. C. H. Steele, in *Proceedings of 2nd International Symposium on Solid Oxide Fuel Cells*, F. Grosz, P. Zegers, S. C. Singhal, and O. Yamamoto, Editors, p. 533, Commission of the European Communities, Report EUR 13546 EN, Luxembourg (1991).
4. T. Kawada, N. Sakai, H. Yokohawa, M. Dokiya, M. Mori, and T. Iwata, *J. Electrochem. Soc.*, **137,** 10 (1990).
5. M. Mogensen, S. Primdahl, J. T. Rheinländer, S. Gormsen, S. Linderoth, and M. Brown, in *Proceedings of 4th International Symposium on Solid Oxide Fuel Cells*, M. Dokiya, O. Yamamoto, H. Tagawa, and S. C. Singhal, Editors, PV 95-1, p. 657, The Electrochemical Society Proceedings Series, Pennington, NJ (1995).
6. S. Primdahl and M. Mogensen, *J. Electrochem. Soc.*, **144,** 3409 (1997).
7. S. Primdahl and M. Mogensen, *J. Electrochem. Soc.*, **145,** 2431 (1998).
8. M. Mogensen and T. Lindegaard, in *Proceedings of 3rd International Symposium on Solid Oxide Fuel Cells*, S. C. Singhal and H. Iwahara, Editors, PV 93-4, p. 913, The Electrochemical Society Proceedings Series, Pennington, NJ (1993).
9. R. J. Aaberg, R. Tunold, S. Tjelle, and R. Ødegård, *High Temperature Electrochemistry: Ceramics and Metals*, 17th Risø International Symposium on Materials Science, F. W. Poulsen, N. Bonanos, S. Linderoth, M. Mogensen, and B. Zachau-Christiansen, Editors, p. 511, Risø National Laboratory, Roskilde, Denmark (1996).
10. S. Sunde, *Electrochim. Acta*, **42,** 2637 (1997).
11. F. Z. Mohamedi-Boulenouar, J. Guindet, and A. Hammou, in *Proceedings of 5th International Symposium on Solid Oxide Fuel Cells*, U. Stimming, S. C. Singhal, H. Tagawa, and W. Lehnert, Editors, PV 97-40, p. 441, The Electrochemical Society Proceedings Series, Pennington, NJ (1997).
12. P. Holtappels, L. G. J. de Haart, and U. Stimming, *J. Electrochem. Soc.*, **146,** 1620 (1999).
13. P. Holtappels, Ph.D. Thesis, Berichte des Forschungszentrums Jülich, Institut für Energieverfahrenstechnik Jül-3414 Julich, Germany (1997).
14. B. A. Boukamp, *Solid State Ionics*, **20,** 31 (1986).
15. J. Völkl and G. Alefeld, in *Hydrogen in Metals I*, G. Alefeld and J. Völkl, Editors, p. 321, Springer Verlag, Berlin (1978).
16. C. Wagner, *Ber. Bunsenges.*, **72,** 778 (1968).
17. V. N. Chebutin, M. V. Glumov, A. D. Neuimin, and S. F. Pal'guev, *Sov. Electrochem.*, **7,** 55 (1971).
18. *Handbook of Chemistry and Physics*, 75th ed., D. R. Lide, Editor, CRC Press, Inc., Boca Raton, FL (1995).
19. M. Mogensen, S. Sunde, and S. Primdahl, *High Temperature Electrochemistry: Ceramics and Metals*, 17th Risø International Symposium on Materials Science, F. W. Poulsen, N. Bonanos, S. Linderoth, M. Mogensen, and B. Zachau-Christiansen, Editors, p. 77, Risø National Laboratory, Roskilde, Denmark (1996).
20. J. R. Macdonald, *Impedance Spectroscopy*, Wiley Interscience, New York (1987).
21. R. D. Armstrong and M. Henderson, *J. Electroanal. Chem.*, **39,** 81 (1972).
22. D. A. Harrington and B. E. Conway, *Electrochim. Acta*, **32,** 1703 (1987).
23. V. N. Chebutin, I. D. Remez, L. M. Solovieva, and S. V. Karpachev, *Electrochim. Acta*, **29,** 1381 (1984).
24. N. L. Robertson and J. N. Michaels, *J. Electrochem. Soc.*, **138,** 1494 (1991).
25. J. Divisek, A. Kornyshev, W. Lehnert, U. Stimming, I. C. Vinke, and K. Wippermann, in *Proceedings of 5th International Symposium on Solid Oxide Fuel Cells*, U. Stimming, S.C. Singhal, H. Tagawa, and W. Lehnert, Editors, PV 97-40, p. 607, The Electrochemical Society Proceedings Series, Pennington, NJ (1997).